Nanoscale

ROYAL SOCIETY OF CHEMISTRY

PAPER

View Article Online
View Journal | View Issue

Cite this: *Nanoscale*, 2022, **14**, 3826

Vibronic effect and influence of aggregation on the photophysics of graphene quantum dots†

Thomas Liu,‡[a] Claire Tonnelé, ‡[b] Shen Zhao,§[a] Loïc Rondin, [a] Christine Elias,[a] Daniel Medina-Lopez,[c] Hanako Okuno,[d] Akimitsu Narita, [e] Yannick Chassagneux,[f] Christophe Voisin, [f] Stéphane Campidelli, [c] David Beljonne [b] and Jean-Sébastien Lauret *[a]

Received 16th December 2021,
Accepted 28th January 2022

DOI: 10.1039/d1nr08279e

rsc.li/nanoscale

Graphene quantum dots, atomically precise nanopieces of graphene, are promising nano-objects with potential applications in various domains such as photovoltaics, quantum light emitters and bio-imaging. Despite their interesting prospects, precise reports on their photophysical properties remain scarce. Here, we report on a study of the photophysics of $C_{96}H_{24}(C_{12}H_{25})$ graphene quantum dots. A combination of optical studies down to the single molecule level with advanced molecular modelling demonstrates the importance of coupling to vibrations in the emission process. Optical fingerprints for H-like aggregates are identified. Our combined experimental–theoretical investigations provide a comprehensive description of the light absorption and emission properties of nanographenes, which not only represents an essential step towards precise control of sample production but also paves the way for new exciting physics focused on twisted graphenoids.

Introduction

Graphene quantum dots (GQDs), the result of the confinement of two-dimensional graphene to a quasi-0D nanostructure, have recently attracted attention for their various promising properties[1–3] and applications including optical-gain media,[4] photovoltaics[5] and bio-imaging.[6] A widely-used route for producing graphene quantum dots is top-down chemistry. Most of the time, these techniques are based on an acid treatment of a graphitic source. They produce suspensions of small pieces of graphene with various uncontrolled shapes, sizes and chemical nature of the edges. As a consequence, their emission properties are dominated by defect states that prevent any study of the properties–structure relationship.[7,8] On the contrary, bottom-up synthesis, where graphene quantum dots are constructed from carefully selected building blocks, allows the production of topologically precise graphenoid nanostructures, where symmetries, size and edges can be perfectly controlled.[9–11] This opened up the way for the specific tailoring of nanostructures according to desired applications, including charge transport[12] or spin properties.[13] Similarly, the energy gap tunability provides a perspective for the control of GQDs' photophysical properties, and the achievement of tunable light sources.[14] Nevertheless, accessing these exciting properties toward the development of devices requires advanced basic studies. Despite the extensive research activities to develop their synthesis, in-depth studies of the photophysical properties of GQDs remain scarce.[15] First, the investigation of GQDs' photophysical properties generally focuses solely on measurements in solution.[16,17] Moreover, extensive theoretical studies on GQDs rarely take vibrational aspects into consideration.[18,19] However, the vibronic coupling is mentioned as a possible reason for the brightening of some dark states, without being formally addressed in the calculations.[26] In this paper, we report on a comprehensive study of the fluorescence of GQDs by a combination of several experimental techniques, including single object spectroscopy and molecular modeling. Here, we focus on $C_{96}H_{24}(C_{12}H_{25})_6$ GQDs (called $C_{96}C_{12}$ hereafter) that are composed of a C_{96} graphenoid core with $C_{12}H_{25}$ alkyl sidechains placed in the periphery to enhance solubility (Fig. 1(a)). We first focus on the spectroscopy of GQD monomers. Then, the effect of aggregation on

[a]*Université Paris-Saclay, ENS Paris-Saclay, CentraleSupélec, CNRS, LuMIn, Orsay, France. E-mail: lauret@ens-paris-saclay.fr*
[b]*CMN, Université MONS, Belgium*
[c]*Université Paris-Saclay, CEA, CNRS, NIMBE, LICSEN, 91191 Gif-sur-Yvette, France*
[d]*University Grenoble Alpes, CEA INAC-MEM, F-38000 Grenoble, France*
[e]*Max Planck Institute for Polymer Research, Ackermannweg 10, 55128 Mainz, Germany*
[f]*LPENS, PSL, CNRS, Université de Paris, Sorbonne Université, 75005 Paris, France*
†Electronic supplementary information (ESI) available. See DOI: 10.1039/d1nr08279e
‡Both authors have the same contribution.
§Current address: Fakultät für Physik, Munich Quantum Center, and Center for NanoScience (CeNS), Ludwig-Maximilians-Universität München, Geschwister-Scholl-Platz 1, 80539 München, Germany.

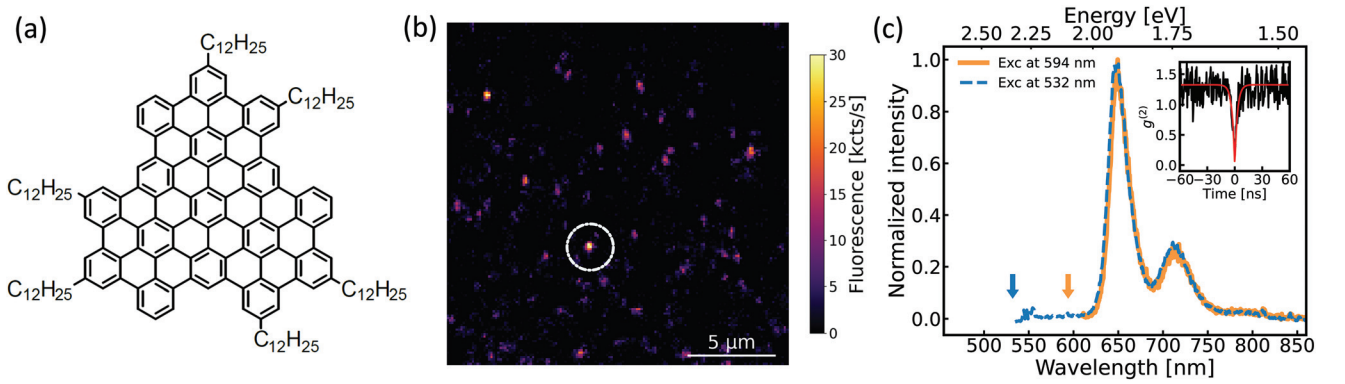

Fig. 1 (a) Chemical formula of the $C_{96}C_{12}$ graphene quantum dots (GQDs). (b) Fluorescence raster scan of the GQD sample recorded by the confocal microscope. The false color represents the fluorescence intensity in kilo counts per second. The dotted white circle highlights a particular spot the spectrum of which is displayed in (c). (c) PL spectrum of a single GQD when excited at 594 nm (in orange) and 532 nm (in blue dashed line). Color arrows indicate the respective excitation wavelengths. Inset: Second-order correlation function $g^{(2)}$ with single-emitter signature ($g^{(2)}(0) < 0.5$).

the optical transitions is investigated, bringing new light on the fluorescence spectrum of an ensemble of GQDs.

Experimental

Synthesis

The details of the synthesis have already been reported.[14,20] Briefly, $C_{96}C_{12}$ GQD is synthesized in two steps from 1,3,5-triethynylbenzene and 2,5-diphenyl-3,4-di(4-dodecylphenyl)-cyclopentadien-1-one, similarly to the literature procedure,[21] *via* Diels–Alder cycloaddition followed by oxidative cyclodehydrogenation in the presence of $FeCl_3$. The intermediate compounds are fully characterized and the GQDs' complete dehydrogenation is checked by MALDI-TOF mass spectrometry (see ESI Fig. S9 and S10†).

Sample preparation

Stock solutions of GQD dispersion with a target concentration of 3×10^{-5} mol L^{-1} were obtained by dispersing GQD powder in 1,2,4-trichlorobenzene (TCB) by stirring for 24 h at room temperature after sonicating the solution for a few seconds (Elma, Elmasonic P). Absorption measurements were directly performed on stock solutions. Stock solutions were then diluted by 100 for fluorescence measurements in solution. In order to prevent any oxygen photo-assisted degradation, the samples are stored in a glovebox under an inert atmosphere (Ar). Samples for single-molecule experiments were obtained by mixing one volume of the diluted GQD solution with one volume of a solution of polystyrene in TCB (at 10% in wt). The solution was spin-coated on a glass coverslip for 180 s at 2000 rpm. Before the spin-coating procedure, the glass coverslip was subjected to 5 minutes of plasma cleaning. The sample was annealed on a hotplate at 90 °C for 1 h.

Optical measurements

Absorption spectroscopy was performed using a commercial spectrometer (PerkinElmer Lambda 950) with 2 mm optical path cuvettes (Hellma Analytics, Quartz Glass High Performance cuvette). Solution PL and PLE measurements were performed using a commercial spectrofluorometer (Horiba, FluoroMax+) with a 10 mm optical path cuvette. Single-molecule measurements were performed using a home-built confocal microscope under ambient conditions. The excitation sources were a continuous-wave diode laser at 594 nm (Cobolt Mambo 100) and a continuous-wave solid-state laser at 532 nm (Sapphire Coherent). The excitation beam was focused onto the sample using an oil-immersion microscope objective (NA = 1.42, Olympus PLAPON 60XO) mounted on a piezoelectric XYZ scanner (Mad City Labs Inc.). Luminescence from the sample was collected in reflection using the same objective, with the excitation beam filtered by a dichroic mirror (zt 594 RDC, Chroma and 552 edge LaserMux, Semrock) and long-pass filters (FELH0600, Thorlabs or 532EdgeBasic, Semrock), and then directed into a spectrometer (SP-2358, Princeton Instruments) coupled with an LN-cooled CCD camera (PyLoN:100BR eXcelon, Princeton Instruments) or into two silicon-based avalanche photodiodes (SPCM-AQR-13, PerkinElmer) mounted in a Hanburry Brown and Twiss configuration. Second-order photon correlation measurements were done using a time-correlated single-photon counting module (PicoHarp300, PicoQuant). A supercontinuum pulsed laser (Fianium), tuned at 580 nm using an acousto-optic tunable filter, was used for lifetime measurements, with a 6 ps pulse width and 60 MHz repetition rate.

Computational details

The $C_{96}C_{12}$ GQD electronic structure and its optical properties have been computed in the gas phase within the framework of the density functional theory (DFT) and time-dependent DFT (TDDFT) using the Gaussian 16 package.[22] The molecular geometry was optimized at the B3LYP/6-31G(d) level. On the basis of this equilibrium structure, the dependence of the excitation energies has been explored for the B3LYP, HSE06, M06-2X, ωB97X-D, and LC-ωPBE (ω = 0.110 $Bohr^{-1}$) exchange–corre-

lation functionals (XCF), and the latter is selected for all TDDFT calculations reported below (see ESI Table S2†). Molecular dynamics (MD) simulations were carried out to investigate the dynamical behavior of GQD monomers and dimers in the 1,2,4-TCB solvent (same as the experiments reported here) using the NAMD code.[23] All simulations started from a low-density box with a 150 Å side and were first equilibrated for 2 ns in the *NpT* isothermal–isobaric ensemble with N being the number of particles, p = 1000 atm, and T = 298.15 K, applying periodic boundary conditions in all three dimensions. In the case of the monomer, the system was further equilibrated for 5 ns at p = 1 atm before a 5 ns production run. For the dimer, an equilibration of 55 ns was performed prior to a 10 ns production run. A time step of 1 fs was used, controlling temperature by rescaling velocities every 100 steps, and pressure with a weak-coupling thermostat. A cutoff radius of 12 Å was employed to truncate the short-range nonbonded interactions, while long-range electrostatic interactions were evaluated through the particle-mesh Ewald method.[24] GQD and solvent molecules were modeled using the General AMBER Force Field[25] (GAFF), with electrostatic potential-fitted partial atomic charges derived from DFT calculations at the B3LYP/6-31G(d) level. To assess the impact of structural dynamics on the optical properties of the $C_{96}C_{12}$ GQD monomer and dimer, TDDFT calculations were performed on 43 and 7 frames extracted from MD simulations, respectively.

Results and discussion

As we have recently demonstrated, $C_{96}C_{12}$ photoluminescence can be addressed at the single object level.[14] This is a critical advantage to probe the intrinsic photophysical properties of these objects. We thus first investigate the photoluminescence properties of an isolated single GQD dispersed in a polystyrene matrix. To identify single GQDs, we first measure the second-order correlation function of photon emission ($g^{(2)}(\tau)$), integrated over the whole spectrum, on a diffraction-limited spot (see Fig. 1(b)). The appropriate antibunching signature ($g^{(2)}(0) < 0.5$, inset of Fig. 1(c)) ensures that a single GQD is addressed. We then measure on such single GQDs, the emission spectrum, under a λ = 594 nm excitation. The orange curve in Fig. 1(c) displays a typical PL spectrum. The characteristic emission lines of a GQD monomer with the main emission peak at around 650 nm are detected. This matches our previous report.[14] The presence of defects in GQDs synthesized by top-down methods results in a fluorescence spectrum that depends on the excitation wavelength.[8] Therefore, to test the presence of higher energy emission lines, we increased the excitation energy (decreased the excitation wavelength to λ = 532 nm) and recorded the spectrum of the very same GQD. As shown in Fig. 1(c), the emission spectrum is not impacted by the excitation wavelength. This observation confirms that the photon emission from this single object results from intrinsic electronic transitions of GQDs and not from a collection of defect states characterized by a wide range of transition energy. In order to get deeper insights into the photophysics, DFT/TDDFT calculations were performed. The first four excited states of the $C_{96}C_{12}$ GQD monomer can be described as combinations of excitations involving doubly degenerate delocalized HOMO and LUMO of e'' symmetry (see Fig. S3† for the description of the orbitals). It results in two low-lying dark states (S_1, S_2) and two degenerate bright states (S_3, S_4) at higher energy (see ESI Table S3†). Interestingly, transitions to S_1 and S_2 are forbidden by the symmetry. It highlights the importance of the shape of GQDs to tailor their properties. The GQD studied here has a C_3 symmetry. A similar behaviour was reported theoretically for GQDs with D_{6h} symmetry, wherein breaking the symmetry leads to a brightening of the two low-energy dark states.[20] More specifically, for the $C_{96}C_{12}$, S_1 and S_3 correspond to the antisymmetric and symmetric linear combinations of HOMO−1 → LUMO and HOMO → LUMO+1 excitations, respectively, while S_2 and S_4 involve the symmetric and antisymmetric combinations of HOMO−1 → LUMO+1 and HOMO → LUMO, respectively. According to Clar's notation for fully benzenoid polycyclic aromatic hydrocarbons (PAHs) like $C_{96}C_{12}$ GQDs, these states can be associated with the α-, p-, and β-bands, in the order of increasing energy.[11] Accounting for the dynamical behavior of the system, an average transition energy of 2.55 eV is computed for the bright states (see the ESI Table S4†). This result fits well with the transition at 478 nm (2.59 eV) measured in optical absorption spectroscopy (see Fig. 4(a) and ESI Fig. S6†). As mentioned above, the two first singlet states are dark by symmetry. Nevertheless, several processes can be at the origin of symmetry breaking as has been observed in many systems.[27–30] In particular, the calculations leading to the forbidden transitions were performed on the planar geometry of the GQD. Interestingly, the transition towards S_2 appears to be partially allowed when the molecular dynamics at room temperature is included in the calculations. Indeed, it gives a non-zero oscillator strength of $f > 0.1$, indicating the coupling of the singlet states to vibrational modes. In particular, low frequency modes that can be associated with the out-of-plane distortion of the nanographene core turn on the $S_0 \rightarrow S_2$ transition. For the sake of illustration, Fig. 2(a) and (b) respectively show a frame obtained in molecular dynamics simulations and the corresponding calculated normal mode. Following the deformation of this mode, the oscillator strength increases and finally exceeds 0.2 (Fig. 2(c)). Surprisingly, and in disagreement with what was expected,[26] we note that such an intensity borrowing effect does not occur for the $S_0 \rightarrow S_1$ transition that is characterized by the vanishing transition densities on all sites, whether the molecule is distorted or not (see ESI Fig. S5†). Fig. 2(c) shows that the excitation energy of the $S_0 \rightarrow S_2$ transition decreases with the increasing deformation amplitude of the considered mode. Therefore, we speculate that this transition either becomes the lowest-lying singlet excited state upon molecular distortion, the state from which the emission occurs, or that $S_0 \rightarrow S_1$ remains the lowest-lying singlet excited state but, being dark, is not observed experimentally. However,

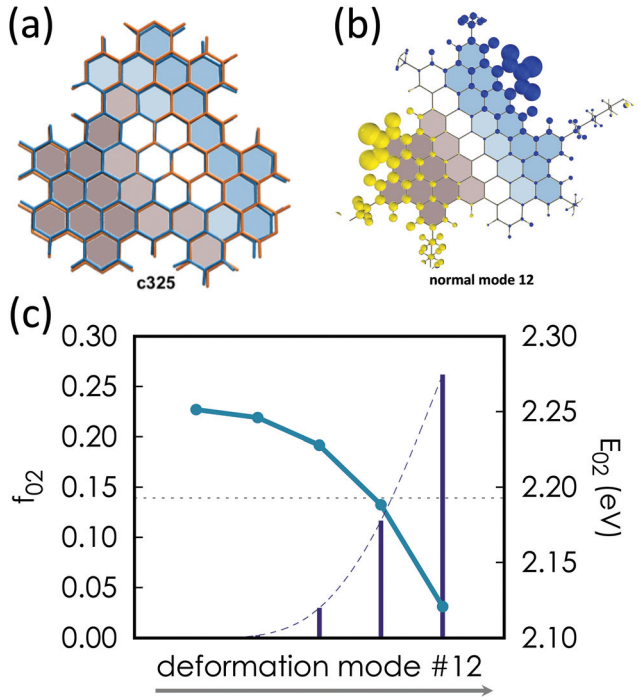

Fig. 2 (a) Deformation patterns for the structure extracted from frame c325 of the molecular dynamics simulations. Colored rings correspond to out-of-plane deformations, upward (dark-grey-filled) or downward (blue-filled) relative to the molecular median plane. (b) Normal mode 12 corresponding to the deformation. (c) Evolution of the oscillator strength and excitation energy of the $S_0 \rightarrow S_2$ transition along the normal mode deformation.

the relatively high fluorescence quantum yield of $C_{96}C_{12}$ ($\geq$35%)[14] does not tally with such a dark state at lower energy than the emissive state, hence we believe the first scenario to be more likely. We note that the lines at lower energies in Fig. 1(c) correspond to vibronic replicas with a quantum of vibration of ~170 meV that is close to the C=C stretching mode energy.

Despite their high interest, one major hurdle of GQDs that slows down basic studies as well as their use in devices is their tendency to aggregate through π–π interactions due to the large size of their sp^2 carbon core. This problem appears clearly while looking at the objects present in the solution. For example, transmission electron microscopy (TEM) reveals lots of small particles (<2 nm), corresponding to individual monomers or a few stacked GQDs dispersed on the graphene support layer as well as columns with few vertically stacked GQDs (see ESI Fig. S11†). Note that such columnar structures have been reported for the specific GQD structure we study here[9] and for other nanographene structures.[31] These observations strongly confirm the existence of H-type aggregates in the solution, with high size dispersion. In this context, we have been looking for a spectral signature of the aggregation in the optical properties of GQDs.

In order to explore the effect of aggregation on the electronic properties, we first extended our calculations on a dimer of $C_{96}C_{12}$. Structurally, the dimer of $C_{96}C_{12}$ GQD presents an H-like configuration with an average interlayer distance of 3.48 Å, indicating π–π interactions within the dimer. The most stable configuration shows a twist angle between the two GQDs of 23° ± 2°. Accordingly, the formation of a dimer is accompanied by a blue-shift of the optical transition by about 30 meV (see ESI Table S5†). The average oscillator strength over the first ten low-lying states amounts to 0.004, which is two orders of magnitude lower than that of the monomer. This should lead to a decrease in fluorescence efficiency in these H-like aggregates. Moreover, we performed the same TDDFT excited-state calculations coupled to MD simulations as done for the monomer in order to probe the effect of lattice fluctuations on the electronic excitations. Compared to the monomer case, the amplitude of the geometric distortions is reduced in the physical dimer. Fig. 3(a) shows the out-of-plane distortion of the GQDs characterized by the branch twist dihedral angle of the GQD branches with respect to the median plane. The distributions of this dihedral angle for a GQD as a monomer and in the dimer are plotted in Fig. 3(b). We observe that the distribution of angles for the monomer is broader than for the GQD in the dimer with a standard deviation of

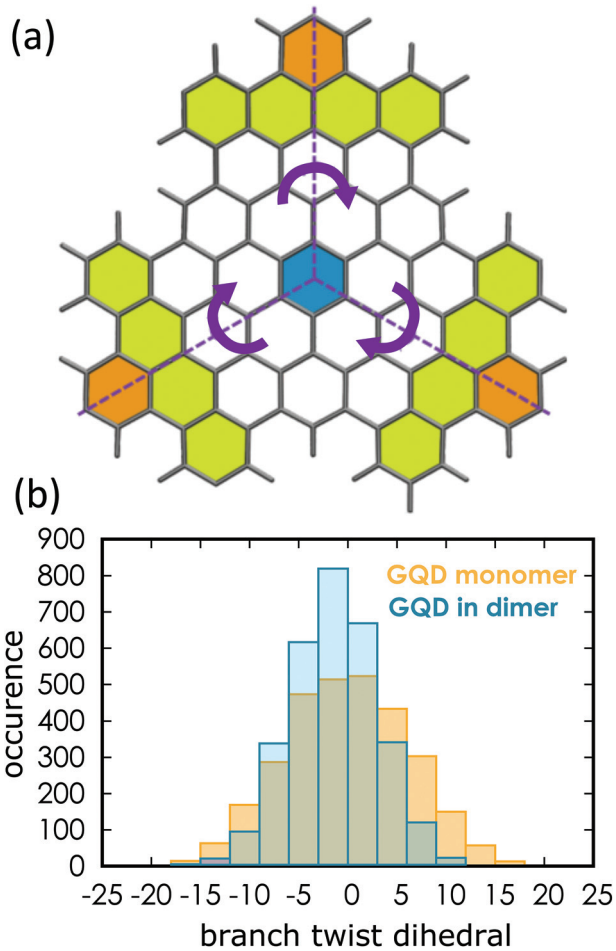

Fig. 3 (a) Out-of plane distortion of the GQDs (b) Distributions of the branch twist dihedral angle of the GQD branches with respect to the median plane: for a monomer (yellow) and for a GQD in a dimer (blue).

σ_{mono} = 6.2° for the monomer *versus* σ_{dimer} = 4.4° and 4.6° for the two GQDs constituting the dimer (see ESI Fig. S4† for the results on the second GQD of the dimer). Most importantly, these structural deformations have a very small impact on the oscillator strength of the lowest-lying states. In summary, these calculations predict that the coupling between monomers in small aggregates leads to a global increase in the energy of the S_0–S_n transition and a decrease in the radiative decay rate from the emissive states.

The UV/visible absorption spectrum of GQD dispersed in 1,2,4-trichlorobenzene (TCB) given in Fig. 4(a) shows broad features typical of large PAHs in solution.[10,32] The main absorption peak is composed of two bands at 455 nm and 475 nm. On the red side of this band, one can observe two other features at 576 nm and 635 nm. This correctly corresponds to the absorption profile previously reported for this specific GQD.[9,14] While the main features of the absorption spectrum are fully reproducible, the details of the structures can vary from one solution to another with more or less pronounced broadening (see ESI Fig. S6†). The fluorescence spectrum of GQDs in the solution is shown in Fig. 4(b). It shows two strong peaks at 644 nm (peak 1) and 703 nm (peak 2), which correctly match the emission lines we previously observed in the single-molecule measurements (see Fig. 1(c)). The energy split between peaks 1 and 2 is ~167 meV, which is also consistent with the vibronic replica observed on the single-molecule spectra. An additional broader band at 577 nm, labeled peak 3, is also noticed. The origin of this higher energy emission peak is yet unclear. First, this high energy line is not detected in the single-molecule measurements reported in Fig. 1(c), excluding the possibility that it arises from intrinsic fluorescence, for instance from a higher singlet state. Therefore, it can be rather related to additional fluorescent species in the solution. This interpretation is strengthened by the time-resolved PL (TR-PL) measurements performed at the wavelengths of peaks 1, 2 and 3, as plotted in Fig. 4(c). The TR-PL spectra collected at 650 nm and 705 nm show the same mono-exponential decay, with a lifetime of ~5 ns, in agreement with experiments on single molecules.[14] The observation of the same dynamics for the emission at the two wavelengths is a solid indication that peaks 1 and 2 in the PL result from the emission of the same object, in our case GQD monomers. The dynamics observed at 575 nm show a multi-exponential decay, with an average shorter fluorescence lifetime. This stark difference in the dynamics confirms that the emission from peak 3 stems from different fluorescent objects.

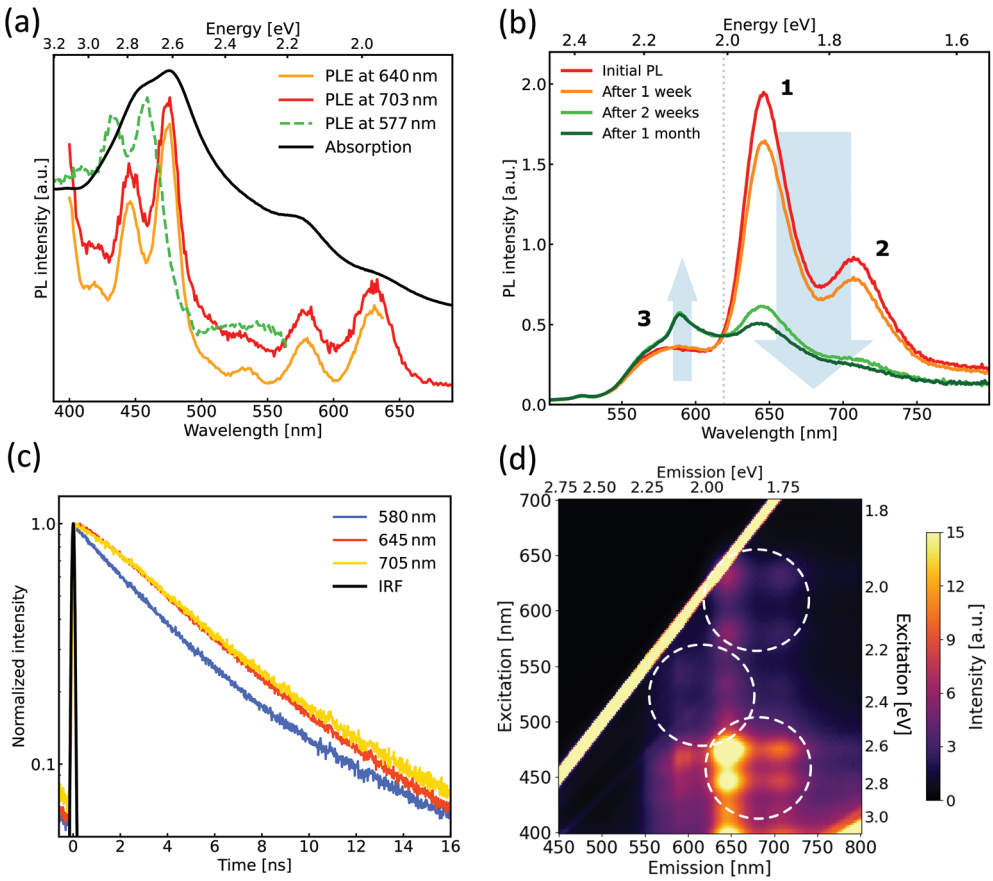

Fig. 4 (a) Absorption spectrum of the $C_{96}C_{12}$ GQD in TCB and PLE spectra collected at the wavelengths of PL peaks 1, 2 (solid lines) and 3 (dashed line). (b) Evolution over time of the fluorescence spectrum of $C_{96}C_{12}$ in TCB. (c) Time-resolved fluorescence spectra detected at the wavelengths of PL peaks 1 (red), 2 (yellow) and 3 (blue) and the (d) PLE 2D map of $C_{96}C_{12}$ in TCB.

As a first hypothesis, synthesis by-products could be considered as a possible origin of this peak. Few impurities, with masses close to the one of $C_{96}C_{12}$, are detected in MALDI-TOF experiments. The different possible structures corresponding to the detected mass are discussed in the ESI.† Nevertheless, Fig. S6† shows that the intensity ratio between PL lines 1 and 3 varies from one suspension to another inside the same batch of GQDs. Making the assumption that the intensities of the PL lines are proportional to the concentrations, this observation demonstrates that the amount of each species varies from one suspension to another, which is unlikely if line 3 would originate only from synthesis by-products. To get more specific insights on the evolution of the fluorescent species population in the solution, we follow its PL time evolution. Fig. 4(b) gives an example of the evolution of the PL spectrum after leaving the sample in an inert Ar environment. We observe that the intensities of peaks 1 and 2 associated with the emission of GQD monomers show a net decrease while the intensity of peak 3 at higher energy increases. In this particular case, an iso-emissive point is observed at 615 nm (see Fig. S7† for other examples). The presence of an iso-emissive point is the signature of a population conversion between the GQD monomers (peaks 1 and 2) and a molecular species emitting at higher energy (peak 3). This again excludes that line 3 arises only from the synthesized by-products. Finally, while the intensity of the fluorescence lines of GQD monomers is reduced by approximately a factor four, the intensity of peak 3 is increased only by a factor ~1.5. It demonstrates that the species the GQD monomers are converted into possess a lower fluorescence quantum yield. This is in line with the decrease in oscillator strength predicted by the calculations. Moreover, the decrease in fluorescence upon aggregation is also commonly observed in other types of chromophores. This is, for instance, one limitation of the efficiency of organic light-emitting diodes.[33] In summary, peak 3 is blue-shifted in comparison to the lines of GQD monomers with a lower quantum yield. Therefore, in line with the theoretical predictions, this line can be related, at least partially, to the emission of small aggregates of $C_{96}C_{12}$ (dimers, trimers...).

Our theoretical calculations indicate that the first four transitions should be blue-shifted upon aggregation. Therefore, we performed PL excitation (PLE) spectroscopy. First, the PLE 2D map is plotted as shown in Fig. 4(d). Some hotspots are observed that are related to resonances between the excited and emissive states. In particular, one can observe the intense spots related to the emission of monomers when excited by the $S_{3,4}$ transitions. Moreover, this 2D map highlights some periodic structures marked by the white dotted circles in the figure. These periodic features are characteristic of the Frank–Condon progression of vibronic replicas. To go into more detail, we focus on the PLE traces detected at several emission wavelengths as displayed in Fig. 4(a). The PLE spectra recorded at 640 nm and at 703 nm lines (emission lines of monomers) present unambiguously the same excitation peaks, which is predictable for PLE spectra originating from the same object. From the lowest to the highest energy, the wavelengths of the lines are: 631 nm, 579 nm, 535 nm, 475 nm, 446 nm, and 420 nm. The energy splits between the three peaks at lower energy and the three peaks at higher energy are respectively, ~176 meV and ~170 meV. These values are again compatible with the C=C vibration energy. This behaviour is fully reproducible from one sample to another. Let us now focus on the high energy emission line 3 at 577 nm. One can see that the excitation energy resonances related to line 3 are blue-shifted by ~100 meV. The blue-shift of the transition, which is fully reproducible, strongly supports the interpretation that line 3 includes a contribution from the emission of small aggregates of $C_{96}C_{12}$ GQDs. Calculations appear to underestimate the blue-shift due to aggregation (30 meV *vs.* 100 meV). This is possibly related to the presence of larger aggregates in the sample than the simple dimers considered in the calculations. Moreover, for this particular sample, the periodic structures in PLE spectra are also observed in emission line 3. From the lowest to the highest energy, the wavelengths of the lines are: 458 nm, 433 nm, and 411 nm. The energy split between these lines is 153 meV, which gives a value lower than that for the lines observed for GQD monomers. This lower value in comparison with the monomer would reflect a decrease in the C=C energy mode in the aggregate. Finally, as for the absorption spectra, the fine structure of the PLE spectra varies for all measured samples. Indeed, for the same powder of GQDs, depending on the suspension process, the blue-shifted PLE spectra show more or less pronounced vibronic progression. The energy shift of the electronic levels, the lowering of the vibration mode and the broadening of the lines originate from the interactions between the monomers inside an aggregate. This interaction is therefore dependent on the details of the structure of the aggregate. Thus, the TEM investigations mentioned previously show that the sample contains aggregates in a H-like configuration with different structures going from two to a dozen layers and with different degrees of disorder. The amount of each type of aggregate depending on the solubilization process, can explain the differences observed from one suspension to another.

Conclusions

In summary, we investigated the photophysics of the $C_{96}C_{12}$ GQDs both at the single-molecule level and in suspension. We demonstrated that the emission spectrum of single GQDs does not depend on the excitation wavelength and arises from intrinsic quantum states. Moreover, calculations showed that the vibrations of the molecular core brighten the second singlet transition while leaving the first one dark. The highlight of the importance of electron–vibration coupling in the emission process suggests digging into this question more deeply. In particular, single-molecule experiments at low temperatures are ongoing. The reduction of the linewidth will enable precise insights into the vibronic coupling in GQDs. Moreover, our results also suggest investigating GQDs with other symmetries, such as D_{2h},[26] but with the same number of

atoms would be very helpful for understanding the structure–properties relationship. Finally, we explored the effect of aggregation on the optical transitions of GQDs. We showed, both theoretically and experimentally, that it leads to a blue shift in the transition and a decrease in the quantum yield. Beyond the better understanding of the photophysics of GQDs, this work opens the way for extensive studies focused on the physics of small aggregates of GQDs that can be viewed as twisted graphenoids.

Author contributions

TL, CE and SZ performed the optical experiments. CT performed the calculations and simulations. DM and SC synthesized and characterized the GQDs. HO performed the TEM measurements. LR, DB and JSL supervised the work and wrote the paper. All the authors participated in the interpretations of the data. TL and CT have equal contributions.

Conflicts of interest

There are no conflicts to declare.

Acknowledgements

This work was financially supported by the FLAG-ERA Grant OPERA by DFG 437130745 and ANR-19-GRF1-0002-01, by the ANR-DFG NLE Grant GRANAO, by DFG 431450789 and ANR-19-CE09-0031-01, and by a public grant overseen by the French National Research Agency (ANR) as part of the "Investissements d'Avenir" program (Labex NanoSaclay, reference: ANR-10-LABX-0035). Computational resources were provided by the Consortium des Équipements de Calcul Intensif (CÉCI), funded by the Fonds de la Recherche Scientifiques de Belgique (F.R.S.-FNRS) under Grant No. 2.5020.11, and the Tier-1 supercomputer of the Fédération Wallonie-Bruxelles. The infrastructure was funded by the Walloon Region under the grant agreement n1117545. D. B. is a FNRS Research Director.

References

1 K. Müllen, *ACS Nano*, 2014, **8**, 6531–6541.
2 J. Wu, W. Pisula and K. Müllen, *Chem. Rev.*, 2007, **107**, 718–747.
3 A. Xu, G. Wang, Y. Li, H. Dong, S. Yang, P. He and G. Ding, *Small*, 2020, **16**, 2004621.
4 G. M. Paternò, Q. Chen, X. Y. Wang, J. Liu, S. G. Motti, A. Petrozza, X. Feng, G. Lanzani, K. Müllen, A. Narita and F. Scotognella, *Angew. Chem., Int. Ed.*, 2017, **56**, 6753–6757.
5 X. Yan, X. Cui, B. Li and L. S. Li, *Nano Lett.*, 2010, **10**, 1869–1873.
6 M. R. Younis, G. He, J. Lin and P. Huang, *Front. Chem.*, 2020, **8**, 1–25.
7 L. Li, G. Wu, G. Yang, J. Peng, J. Zhao and J. J. Zhu, *Nanoscale*, 2013, **5**, 4015–4039.
8 Q. Xu, Q. Zhou, Z. Hua, Q. Xue, C. Zhang, X. Wang, D. Pan and M. Xiao, *ACS Nano*, 2013, **7**, 10654–10661.
9 Ž. Tomović, M. D. Watson and K. Müllen, *Angew. Chem., Int. Ed.*, 2004, **43**, 755–758.
10 X. Yan, X. Cui and L. S. Li, *J. Am. Chem. Soc.*, 2010, **132**, 5944–5945.
11 R. Rieger and K. Müllen, *J. Phys. Org. Chem.*, 2010, **23**, 315–325.
12 M. Imran, C. M. Wehrmann and M. S. Chen, *J. Am. Chem. Soc.*, 2020, **142**, 38–43.
13 F. Lombardi, A. Lodi, J. Ma, J. Liu, M. Slota, A. Narita, W. K. Myers, K. Müllen, X. Feng and L. Bogani, *Science*, 2019, **366**, 1107–1110.
14 S. Zhao, J. Lavie, L. Rondin, L. Orcin-Chaix, C. Diederichs, P. Roussignol, Y. Chassagneux, C. Voisin, K. Müllen, A. Narita, S. Campidelli and J.-S. Lauret, *Nat. Commun.*, 2018, **9**, 3470.
15 M. Semeniuk, Z. Yi, V. Poursorkhabi, J. Tjong, S. Jaffer, Z.-H. Lu and M. Sain, *ACS Nano*, 2019, **13**, 6224–6255.
16 M. L. Mueller, X. Yan, J. A. McGuire and L.-S. Li, *Nano Lett.*, 2010, **10**, 2679–2682.
17 S. Zhu, L. Wang, B. Li, Y. Song, X. Zhao, G. Zhang, S. Zhang, S. Lu, J. Zhang, H. Wang, H. Sun and B. Yang, *Carbon*, 2014, **77**, 462–472.
18 H. Riesen, C. Wiebeler and S. Schumacher, *J. Phys. Chem. A*, 2014, **118**, 5189–5195.
19 Y. Li, H. Shu, S. Wang and J. Wang, *J. Phys. Chem. C*, 2015, **119**, 4983–4989.
20 V. S. Iyer, M. Wehmeier, J. D. Brand, M. A. Keegstra and K. Müllen, *Angew. Chem., Int. Ed. Engl.*, 1997, **36**, 1604–1607.
21 M. Wehmeier, M. Wagner and K. Müllen, *Chemistry*, 2001, **7**, 2197–2205.
22 M. J. Frisch, G. W. Trucks, H. B. Schlegel, G. E. Scuseria, M. A. Robb, J. R. Cheeseman, G. Scalmani, V. Barone, G. A. Petersson, H. Nakatsuji, X. Li, M. Caricato, A. V. Marenich, J. Bloino, B. G. Janesko, R. Gomperts, B. Mennucci, H. P. Hratchian, J. V. Ortiz, A. F. Izmaylov, J. L. Sonnenberg, D. Williams-Young, F. Ding, F. Lipparini, F. Egidi, J. Goings, B. Peng, A. Petrone, T. Henderson, D. Ranasinghe, V. G. Zakrzewski, J. Gao, N. Rega, G. Zheng, W. Liang, M. Hada, M. Ehara, K. Toyota, R. Fukuda, J. Hasegawa, M. Ishida, T. Nakajima, Y. Honda, O. Kitao, H. Nakai, T. Vreven, K. Throssell, J. A. Montgomery Jr., J. E. Peralta, F. Ogliaro, M. J. Bearpark, J. J. Heyd, E. N. Brothers, K. N. Kudin, V. N. Staroverov, T. A. Keith, R. Kobayashi, J. Normand, K. Raghavachari, A. P. Rendell, J. C. Burant, S. S. Iyengar, J. Tomasi, M. Cossi, J. M. Millam, M. Klene, C. Adamo, R. Cammi, J. W. Ochterski, R. L. Martin, K. Morokuma, O. Farkas, J. B. Foresman and D. J. Fox, *Gaussian 16, Revision B.01*, 2016.

23 J. C. Phillips, R. Braun, W. Wang, J. Gumbart, E. Tajkhorshid, E. Villa, C. Chipot, R. D. Skeel, L. Kalé and K. Schulten, *J. Comput. Chem.*, 2005, **26**, 1781–1802.
24 U. Essmann, L. Perera, M. L. Berkowitz, T. Darden, H. Lee and L. G. Pedersen, *J. Chem. Phys.*, 1995, **103**, 8577–8593.
25 J. Wang, R. M. Wolf, J. W. Caldwell, P. A. Kollman and D. A. Case, *J. Comput. Chem.*, 2004, **25**, 1157–1174.
26 C. Cocchi, D. Prezzi, A. Ruini, M. J. Caldas and E. Molinari, *J. Phys. Chem. A*, 2014, **118**, 6507–6513.
27 F. Terenziani, A. Painelli, C. Katan, M. Charlot and M. Blanchard-Desce, *J. Am. Chem. Soc.*, 2006, **128**, 15742–15755.
28 F. Terenziani, C. Sissa and A. Painelli, *J. Phys. Chem. B*, 2008, **112**, 5079–5087.
29 W. Verbouwe, M. Van der Auweraer, F. C. De Schryver, J. J. Piet and J. M. Warman, *J. Am. Chem. Soc.*, 1998, **120**, 1319–1324.
30 B. Dereka, D. Svechkarev, A. Rosspeintner, A. Aster, M. Lunzer, R. Liska, A. M. Mohs and E. Vauthey, *Nat. Commun.*, 2020, **11**, 1925.
31 X. Feng, V. Marcon, W. Pisula, M. Ryan Hansen, J. Kirkpatrick, F. Grozema, D. Andrienko, K. Kremer and K. Müllen, *Nat. Mater.*, 2009, **8**, 12.
32 J. A. McGuire, *Phys. Status Solidi RRL*, 2016, **10**, 91–101.
33 K. Zhang, J. Liu, Y. Zhang, J. Fan, C.-K. Wang and L. Lin, *J. Phys. Chem. C*, 2019, **123**, 24705–24713.